A Comparison Between Highly Crystalline and Low Crystalline Poly(phenylene sulfide) as Polymer Electrolyte Membranes for Fuel Cells

Mohammad A. Barique,*,† Surasak Seesukphronrarak,† Libin Wu,†,§ and Akihiro Ohira*,†,‡

Polymer Electrolyte Fuel Cell Cutting-Edge Research Center (FC-Cubic), Technology Research Association, 2-3-26 Aomi, Koto-ku, Tokyo 135-0064, Japan, and Research Institute for Ubiquitous Energy Devices, National Institute of Advanced Industrial Science and Technology (AIST), Midorigaoka, Ikeda, Osaka 563-8577, Japan

Received: September 8, 2010; Revised Manuscript Received: November 26, 2010

Sulfonation-induced changes in the crystalline structures of highly crystalline (HC) and low crystalline (LC) poly(phenylene sulfide) (PPS) electrolyte membranes and relative humidity-induced changes in the morphology of those sulfonated PPS (SPPS) membranes were characterized by wide-angle X-ray scattering, small-angle X-ray scattering, and atomic force microscopy. The correlations between the hydrated morphology and the development of proton channels in both kinds of membranes are discussed in the paper. For HC-PPS membranes, crystallinity decreased steeply up to an ion-exchange capacity (IEC) of 1.6 meq/g during sulfonation, but in the case of LC-PPS membranes, crystallinity decreased up to IEC = 0.9 meq/g, but not as steeply as for HC membranes. In the varied hydration conditions of the membranes, water molecules were not predominately located within the ionic aggregation but, rather, were gradually dispersed and rearranged through the whole membrane with increasing hydration level. For both kinds of membranes, HC-SPPS and LC-SPPS, Porod plots showed a "positive deviation" that revealed that the polymer/water interface under varied hydration conditions was not smooth, but diffused, and well-developed proton channels did not form in the membranes. LC-SPPS membranes showed about a 10% rougher (from α value) polymer/water interface than HC-SPPS membranes.

Introduction

Fuel cells have received considerable attention as electrical power sources during the 21st century because of their high efficiency and low pollution levels.[1−3] A polymer electrolyte membrane (PEM) in a membrane electrode assembly (MEA) of a polymer electrolyte fuel cell (PEFC) acts as an electrolyte medium for proton (H^+) transport and prevents fuel crossover. For the past few years, alternative membranes to the widely known Nafion have been developed with nonperfluorinated backbone chains. PEMs based on aromatic hydrocarbon polymers are attractive for a variety of reasons, including potentially lower cost, easier processing, and higher operating temperatures. Various membranes based on sulfonated high-performance aromatic hydrocarbon polymers have been shown to be attractive alternatives to Nafion because of their high inherent stability and high glass transition temperatures.[4,5] It is necessary to improve proton conductivity especially under low-humidity conditions at high operating temperatures to improve the current aromatic PEM system.[6] The changes in crystal morphology induced by sulfonation played a significant role in the regulation of proton transport.[7] Still now, there are very few reports on the mechanism of the sulfonation process in hydrocarbon membranes with varied crystallinity and the development of proton channels in those sulfonated structures in hydration conditions. The degree of crystallinity and orientation of the crystalline domains are important factors in controlling the physical properties of the membrane, and many efforts have been devoted to the understanding of the crystallization and orientation behavior of polymers in one-,[8−11] two-,[12−21] or three-dimensional[22−25] confinements.

SCHEME 1: Chemical Structures of PPS and Sulfonated PPS (SPPS)

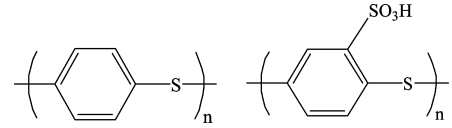

In the present work, we utilized a PPS hydrocarbon polymer as an electrolyte membrane material, which is an engineering thermoplastic and has found numerous uses due to its excellent combination of properties, including good mechanical and high thermal stability, high glass transition temperature, chemical resistance, flame resistance, and excellent process ability. The basic molecular structure of PPS is a series of alternating para-substituted phenylene rings and divalent sulfide moieties, as shown in Scheme 1.[26]

The semicrystalline morphology of PPS is described in terms of a three-phase system comprising a crystalline phase, a mobile amorphous phase, and a rigid amorphous phase.[27] In our preceding paper,[28] we reported the effect of water on the changes in morphology and proton conductivity of highly crystalline PPS electrolyte membranes. In the present paper, we report the fundamental study on the comparison of sulfonation-induced changes in crystalline morphology, the correlations between morphology and ion−water aggregation for developing proton channels, and the proton conductivity of HC- and LC-SPPS membranes in varied hydration conditions.

* To whom correspondence should be addressed. Tel: +81 3 3599 8550. Fax: +81 3 3599 8554. E-mail: ma.barique@fc-cubic.or.jp (M.A.B.), a-oohira@aist.go.jp (A.O.).

† Polymer Electrolyte Fuel Cell Cutting-Edge Research Center (FC-Cubic), Technology Research Association.

‡ Research Institute for Ubiquitous Energy Devices, National Institute of Advanced Industrial Science and Technology (AIST).

§ Present address: Dept. Organic and Polymeric Materials, Tokyo Institute of Technology, Ookayama 2-12-1-S5-20, Meguro-ku, Tokyo, 152-8552, Japan.

10.1021/jp108562s
Published on Web 12/15/2010

Experimental Section

Sulfonation of PPS Membranes.

HC-PPS. The sulfonation of commercial HC-PPS membranes (thickness = 50 μm) of 82% crystallinity was performed by the following procedure.[29] A 50 g portion of dichloromethane and 0.117 g of chlorosulfonic acid were weighed and put in a 50 mL glass flask to prepare a chlorosulfonic acid solution. A 0.117 g portion of PPS membrane was weighed, immersed in the chlorosulfonic acid solution, and left for 20 h at room temperature. The sulfonated PPS membrane was then recovered from the solution and rinsed with deionized water until it became neutral. The SPPS membrane was again immersed in 50 mL of deionized water and left for 20 h at room temperature. The membrane was recovered and dried under reduced pressure at 80 °C for 3 h. The IEC value of the membrane was then determined by back-titration. Other higher IEC value membranes were prepared in the same procedure by gradual increase of the amount of chlorosulfonic acid.

LC-PPS. The sulfonation of commercial LC-PPS membranes (thickness = 50 μm) of 42% crystallinity was performed using the same procedure described above for the HC-PPS membrane.

Titration Procedure. The IEC value for each SPPS membrane was determined through the back-titration method. SPPS membranes in acid (H^+) form were dried overnight at 100 °C under vacuum, weighed, and then immersed in saturated NaCl for 24 h. The amount of H^+ ion released from the membrane samples was determined by titration with 0.01 M NaOH using phenolphthalein as an indicator. The IEC value of the SPPS membranes was calculated with the following equation

$$\mathrm{IEC} = \frac{CxV}{M} \qquad (1)$$

where C and V are the concentration and volume of NaOH, respectively, and M is the weight of the membrane.

Measurements

WAXS. WAXS was measured to analyze the crystalline morphology of the HC- and LC-SPPS membranes using a Rigaku Ultima-IV X-ray diffractometer with Ni-filtered Cu Kα radiation (λ = 0.15418 nm) operated at 40 kV and 40 mA in air, in symmetrical reflection mode. The X-ray profiles were taken at room temperature using a scintillation counter operated in a stepping mode with a sample-to-detector distance of 30 cm, and samples were scanned at diffraction angles in the 2θ range of 5−90° with a step scan interval of 0.2°/min. The intensity profiles were smoothed, and the background (dark scattering) was subtracted from every profile.

SAXS. Point-collimated SAXS measurements were carried out using a NANO-Viewer (Rigaku Corporation) with Ni-filtered Cu Kα radiation (λ = 0.15418 nm) that was finely focused by a confocal max-flux mirror (CMF) and collimated into the Rigaku-made airtight sample chamber with Kapton windows using a three-slit system. The chamber was then connected with a humidity generator (model HUM-1) under ambient conditions of temperature and relative humidity (RH). The size of the X-ray beam was 0.07 × 0.7 mm^2; the widths of the three slits were 0.4, 0.2, and 0.6 mm; and SAXS was operated at 40 kV and a 30 mA power beam. Two-dimensional SAXS patterns were recorded on a sheet of an imaging plate (IP) by the transmission method, and the sample-to-IP distance was set at 60 cm. X-ray scattering patterns were recorded for 6 h at 40 °C for every constant RH. Scattered intensity $I(q)$ values from all the SAXS image patterns were corrected by subtracting the air and dark scattering. $I(q)$ values were recorded in steps of scattering vector $q = (4\pi \sin\theta)/\lambda$, where q is the phonon vector, 2θ the scattering angle, and λ the X-ray wavelength.

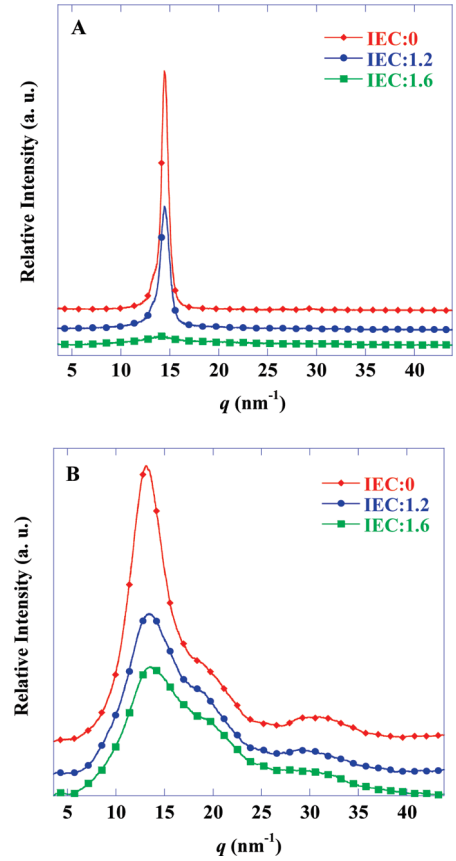

Figure 1. WAXS profiles for (A) HC-SPPS and (B) LC-SPPS membranes with varied IECs. For HC-SPPS, the WAXS intensity is almost diminished, but for LC-SPPS, the WAXS intensity does not diminish with increasing IEC.

AFM Observation. ac-mode AFM and current-mapping images were obtained using a JSPM-5400 (Nihon Denshi) with a humidity control unit. A Pt-coated cantilever (TAP-300E, BudgetSensors) with a force constant of 40 N/m and a resonance frequency of 300 kHz was used. Membrane samples were placed on a gold-plated conductive sample stage with Nafion dispersion (DE-2020, DuPont) as an adhesive. Before AFM observation, the sample was placed in a humidity-controlled chamber for at least 3 h. A bias voltage was applied to the sample stage during observation. All the topography, phase, and current mapping images were obtained simultaneously.

Results and Discussion

Influence of Sulfonation Level on the Changes in Crystalline Morphology of HC- and LC-PPS Membranes. It is essential to understand the influence of the sulfonation level on the morphology of the original polymer matrix to control the desired properties of the final PEM. The most important changes with respect to the sulfonation level are the changes in crystalline morphology (size, shape, and state of dispersion of crystallites), crystallinity, and chain extension.[30] The effects of the sulfonation level on changes in the structure and morphology of PPS crystallites was studied by WAXS. Figure 1A,B shows the effect of sulfonation level on the WAXS intensity for HC- and LC-SPPS membranes. For HC-SPPS membranes, a strong and sharp peak at 14.51 nm^{-1} (Figure 1A) was found, which arose from

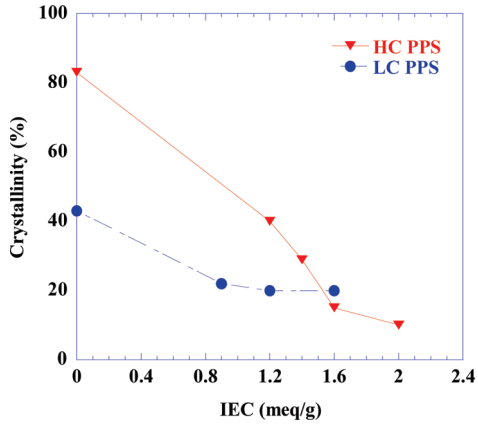

Figure 2. Dependence of crystallinity on the IEC for HC- and LC-SPPS membranes. For HC-PPS membranes, crystallinity reaches equilibrium after an IEC level of 1.6, but for LC-PPS membranes, the same phenomenon occurs after IEC = 1.2.

the convolution of lamellar and amorphous scattering.[31] The peak arises from the (110) plane of the orthorhombic PPS structure.[32,33] With increasing the sulfonation level, the peak intensities were reduced but the diffraction peaks were still preserved even at an IEC of 2.0, indicating that, though very small, the main crystallite was retained. The results indicated that, though the HC-SPPS membranes lost their three-dimensional (3D) crystal structure after a sufficient degree of sulfonation, a two-dimensional (2D) ordered structure was still retained.[34] For LC-SPPS membranes (Figure 1B), the crystalline peak from (110) arose at 13.16 nm^{-1} and two other very broad peaks also appeared at 18.63 and 30.58 nm^{-1}, arising from two different planes composed of very small crystallites oriented in different directions, and those broad peaks were absent in HC membranes. The broad peak widths indicated the low crystallinity (amorphous nature) of the membranes.

The above results indicated that HC-PPS has only a main plane of (110) but LC-PPS have smaller crystals oriented in different planes with different directions of polymer chains. In the case of HC-SPPS membranes, the scattering intensity decreased very dramatically with increasing IEC, and the peak profiles became gradually very broad and finally nearly diminished. Unlike HC-SPPS membranes, in the case of LC-PPS membranes, the intensity gradually decreased but the peak profiles did not diminish with increasing IEC. It has been reported that the sulfonation of poly ether ketone ketone (PEKK) decreased its crystallinity with the sulfonation level increased, as shown by the loss of crystalline reflections in the WAXD profiles.[34] A similar effect has also reported for the sulfonation of PEEK.[35]

The effect of sulfonation level (IEC) on the degree of crystallinity (χ_c) for HC- and LC-SPPS membranes was extracted from the WAXS profiles (Figure 1A,B), and is shown in Figure 2. The degree of crystallinity for varied IEC SPPS membranes was calculated from their WAXS profiles with the following equation

$$\chi_c = 1 - \frac{I_a}{(I_a + I_c)} \qquad (2)$$

where χ_c refers to the degree of crystallinity, I_c refers to the integrated value of the scattering intensity of the crystalline volume, and I_a refers to the integrated intensity of the amorphous volume fraction of the sample.

TABLE 1: Effect of IEC (Sulfonation Level) on Crystallite Size and Interdomain Spacing in SPPS Membranes

IEC (meq/g)	crystallite domain size (nm)		interdomain spacing (nm)	
	HC-PPS	LC-PPS	HC-PPS	LC-PPS
0	12	1.41	0.43	0.48
1.2	5	0.72	0.43	0.46
1.6	2	0.60	0.44	0.46

A remarkable difference in the decreasing tendency of crystallinity for the both kinds of membranes was observed. It was noticed that the HC-SPPS membranes showed a steep decrease in crystallinity until an IEC level of 1.6, and after that, crystallinity does not decrease appreciably with increasing the sulfonation level. However, in the case of LC-SPPS membranes, the decrease in crystallinity was not steep at all and crystallinity decreased slightly until IEC = 1.2, and after that, it did not decrease further. We consider the crystallite domain in the crystalline regions of the PPS membrane as a core−shell model;[28] sulfonation initially starts to attach the sulfonic acid group (−SO_3H) to the phenylene rings of the outside amorphous chains (the shell) of the system and gradually proceeds to the depth of the membrane with rupturing the crystallite domains (the core). We suggest that, in the case of HC-PPS, the sulfonation proceeds through the above process and destroys almost all the lamellar crystallites with increasing sulfonation level, but a small amount of tightly packed crystalline seeds still remain even at higher IEC, which were detected by WAXS (Figure 1A). As the polymer chains in lamellar crystallites in the HC-PPS membrane are in a statistically arranged and close-compact condition, the sulfonation proceeds smoothly and aggressively to the depth of the membrane as much as possible, making the chains amorphous. Thus, the amorphous volume increases with the chain extension and the crystallinity decreases rapidly. In the case of LC-PPS, from the beginning, the membrane has only a 42% crystallinity volume; that is, a larger volume of the membrane is amorphous. The total amount of arranged and closely packed chains is less; because the chains are arrayed randomly throughout the membrane and there is a lesser amount of crystallites to be sulfonated, the sulfonation proceeds randomly. As a result, the crystallinity does not decrease so steeply like HC-PPS. Although the IEC value increases with increasing the number of attached SO_3H groups in the randomly arrayed chains, the crystallinity does not decease so much. Therefore, the crystallinity for the same IEC values is different for HC-SPPS and LC-SPPS membranes with an IEC less than 1.2. Furthermore, in case of HC-PPS membranes after an IEC level of 1.6, the membrane become amorphous due to sufficient sulfonation, and the benzene rings to be sulfonated become less accessible due to the tiny rigid crystallites left. Consequently, the crystallinity does not decrease and reaches equilibrium, even though the sulfonation proceeds slowly with increasing IEC. For LC-PPS membranes, the same phenomenon occurs after IEC = 1.2.

The effect of sulfonation on the crystallite size and their interdomain spacing for HC- and LC-SPPS membranes are shown in Table 1. The crystallite domain size D_{hkl} was calculated from the (110) peak using the Scherrer equation

$$D_{hkl} = \frac{\lambda}{\beta_{hkl} \cos \theta_{hkl}} \qquad (3)$$

where λ is the X-ray wavelength, β_{hkl} is the full width at half-maximum (fwhm) of the profiles (after correction for apparatus

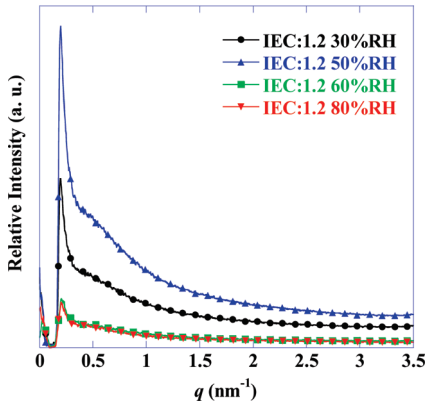

Figure 3. SAXS profiles for HC-SPPS membranes with IEC = 1.2 for varied RHs. The incident X-ray beam was normal to the film surface. The SAXS shoulder peak intensity at 0.5 nm^{-1} gradually increased up to 50% RH and then decreased gradually with increasing RH.

broadening), and θ is the Bragg angle of the *hkl* reflection. It was found that the crystallite size decreases with increased sulfonation level for both kinds of membranes. The average crystallite domain size in HC-SPPS is several times larger than the crystallite in the LC-SPPS membrane of the same IEC value. We suggest that the appreciably larger crystallite size and high crystallinity cause the steep decrease in crystallinity in HC-PPS during sulfonation. From Table 1 for HC-SPPS, it was found that at IEC = 1.6, the average crystallite size is 2 nm and, at this stage, the sulfonation reaches equilibrium. For LC-PPS, it was found that the crystallite domain size from the beginning is very small; at IEC = 1.2, the size is only 0.7 nm and the reaction reaches equilibrium here. That may be the reason why the sulfonation in LC-PPS reaches equilibrium comparatively earlier than in HC-PPS.

Morphology of HC- and LC-SPPS Membranes with Varied Water Contents and IECs Studied by SAXS. The exact hydrated morphology of hydrocarbon membranes is still not completely understood, although in our previous paper,[28] we proposed a schematic diagram to explain the morphology in varied water contents for highly crystalline PPS membranes, which gave a basic image of states of ion−water aggregates in hydrocarbon PEMs. The hydrated morphology and development of microphase separation between the hydrophobic PPS backbone matrix and the hydrophilic SO_3H ionic sites in HC- and LC-SPPS membranes were studied by SAXS. Figures 3 and 4 show the effect of RH on the SAXS profiles for varied IEC SPPS samples measured at 40 °C. HC-SPPS and LC-SPPS exhibited remarkable differences in their SAXS intensity with respect to *q*, which indicated that two different types of hydrated morphologies developed in the membranes. Figure 3 shows the effect of RH on the SAXS intensity for HC-SPPS membrane with IEC = 1.2. A broad shoulder peak in the SAXS profile at around 0.5 nm^{-1} was observed, and the origin of this peak is the electron density difference between the lamellar crystallite domains and the amorphous domains in the membrane.[36]

From Figure 3, it was observed that the SAXS intensity gradually increases with increasing RH and reaches a maximum at 50% RH and, after that, the intensity gradually starts to decrease and finally decreases to even less than at 30% RH. A similar trend was found for other highly crystalline PPS membrane samples with varied IECs, which is published in our previous paper.[28] Figure 4A−C shows the SAXS intensity profiles for IEC values of 0, 1.2, and 1.6, respectively, for LC-SPPS membranes at varied RHs. It was observed that the SAXS intensity does not increase with increasing RH over the whole

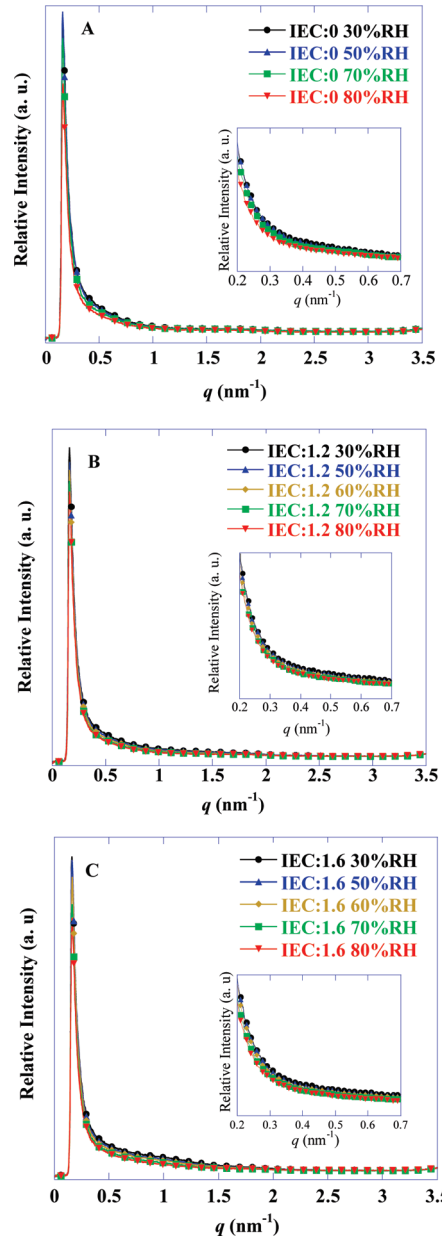

Figure 4. SAXS profiles for LC-SPPS membranes with (A) IEC = 0, (B) IEC = 1.2, and (C) IEC = 1.6 for varied RHs. The incident X-ray beam was normal to the film surface. No shoulder peak appeared in the SAXS profiles due to the low crystallinity of LC-SPPS membranes.

q region; rather, the scattering intensity gradually decreases monotonously with increasing RH from the beginning. All the LC-SPPS samples with varied IECs showed similar results. We suggest that, in the case of the HC-SPPS membrane, some SO_3H−water aggregates form in the amorphous domains at lower RH and these ion−water aggregates become gradually larger with an increasing amount of water in the membrane, and at around 50% RH, the aggregates size becomes maximum. As a result, the SAXS intensity at 0.5 nm^{-1} from the water-absorbed amorphous domains becomes higher. However, after that, those ion−water aggregates gradually start to disperse with an increasing amount of water in the membrane. For HC-SPPS, we consider that, above 50% RH, the water−water hydrogen bonds become stronger than the ion−water attraction in the amorphous domains, which results in the dispersion of the ion−water aggregates and causes the decrease of the SAXS shoulder peak intensity. In the case of LC-SPPS membranes

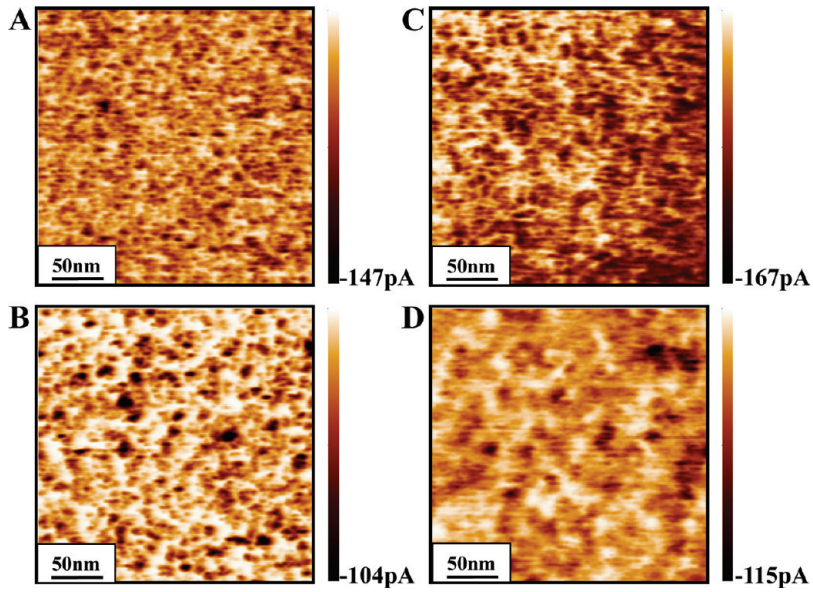

Figure 5. ac-AFM current-mapping images of SPPS membranes at 21 °C and 85% RH: (A) HC-SPPS, IEC = 1.2; (B) LC-SPPS, IEC = 1.2; (C) HC-SPPS, IEC = 1.4; and (D) LC-SPPS, IEC = 1.3. Scan size: 250 nm × 250 nm. Scan rate: 1.5 Hz. Applied bias voltage: (A) −2.4, (B) −2.5, (C) −1.8, and (D) −2.0 V.

with varied IECs, no water aggregates develop with increasing RH; rather, the water starts to disperse from the beginning. We suggest that the size of the water absorbed amorphous domains is the factor responsible for developing the ion−water aggregates in the sulfonated membranes.

In general, when the hydrophobic and hydrophilic phases are partially or completely phase-separated, a peak from ion−water aggregates appears in the large q region of the SAXS profile. The SAXS pattern of the Nafion membrane is known to consist of two peaks, one in the low-q region and other in the high-q region. The latter ionomer peak (in the high-q region) is generally ascribed to the distribution of ionic clusters in the membrane, whereas the low-q peak is ascribed to the long-range crystalline domains of a lamellar structure in the matrix.[37] However, no absolute peak from ion−water aggregations appeared in the SAXS profiles in Figures 3 and 4 for any IEC samples of HC- and LC-SPPS membranes. This indicates that the rigid backbone of PPS restricts the molecular mobility and rearrangement of main chains in both HC- and LC-SPPS membranes even at higher water content and higher IEC, so no remarkable ion−water aggregations or clusters develop, which can give rise to a peak in the SAXS profile. The SO_3H groups in the membranes are just statistically and randomly attached in the phenylene rings of the PPS main chain and lack plasticity. Also, due to the absence of a side chain, SO_3H ions have no chance of any displacement that can develop ion−water aggregates. Although the amount of water increases in the membrane, the water just spread through the membrane without forming any larger ion−water aggregates that can phase separate. On the other point of view, according to Fujimura et al., the absence of a SAXS peak does not necessarily exclude the possibility of ionic aggregation. It is possible for the aggregation to be present without giving rise to a SAXS peak, if the contrast (electron density difference) between ion-rich and ion-poor regions is too low.[38,39]

AFM observation can lead to analyzing the proton transport ability in membranes from a macroscopic point of view. Figure 5 shows the ac-mode current-mapping AFM images at 21 °C and 85% RH for HC- and LC-SPPS membranes. The dark areas correspond to hydrophilic (SO_3H) regions where a proton passes through the membrane, and the bright areas correspond to hydrophobic (PPS matrix) regions. From all of the images in Figure 5, no larger ion−water aggregate or proton channel network could be observed. This result implies that the adsorbed water molecules are not conglomerated locally but are distributed homogeneously in the membrane with increasing water uptake. However, some differences between the surface morphology for the same IEC HC- and LC-SPPS membranes at 85% RH could be observed. On comparison of the current maps of HC- and LC-SPPS membranes with IEC = 1.2 (Figure 5A,B), it can be observed that HC-SPPS (Figure 5A) has a higher ion−water aggregate density with short-range cocontinuous ion−water aggregations connected for proton passing than LC-SPPS (Figure 5B). Again, comparing HC-SPPS with IEC = 1.2 (Figure 5A) and IEC = 1.4 (Figure 5C), we can observe that, with increasing IEC, the aggregates became larger and continuous and, in some parts of the membrane, the proton-conducting region became remarkably larger. In the case of LC-SPPS, comparing panels B and D in Figure 5, we observed that, with increasing IEC, the proton conductive regions did not become large, though the aggregates swell and become slightly larger, but the tendency was not like HC-SPPS.

States of the Polymer/Water Interface at Varied RHs and IEC for HC- and LC-SPPS Membranes. The state of the polymer/water interface is the key issue to develop the proton channel in the sulfonated membranes.[28] Proton transport can be regarded primarily as an interfacial phenomenon at the water/polymer interface, with lots of ramifications due to the complex random structure of the interface and complex interactions in the polymer/water system. These effects become increasingly important with decreasing water content.[40] The states of polymer/water interface sharpness and the developing process for ion−water aggregates were analyzed by the Porod plot from the SAXS data for every IEC of HC- and LC-SPPS membranes. The intercept slope (α) values were deduced from the high-q region of SAXS profiles for the HC and LC membranes, and the results are shown in Table 2. Generally, the α value of −4 from the equation, $I(q) \propto q^{-4}$, indicates a sharp interface and the presence of phase separation of a two-phase system.[41] From Table 2, it was found that there is very little difference in slope

TABLE 2: Porod Slope Values (α) for the HC- and LC-SPPS Membranes for Varied IECs and RHs

	IEC:1.2		IEC:1.6
	HC	LC	LC
RH (%)	α	α	α
30	−6.2	−6.8	−6.6
50	−6.3	−6.8	−6.5
60	−6.2	−6.7	−6.5
70		−6.6	−6.3
80	−6.4	−6.6	−6.2

values of HC- and LC-SPPS membranes for the same IEC membrane. Also, for the all IECs, the slope values were very similar. All the values were around −6, which indicated that the polymer/water interface was not sharp, but remarkably diffused. A three-dimensional (3D) schematic model of states of ion−water aggregates in the HC- and LC-SPPS membranes with varied hydration levels is illustrated in Scheme 2.

Gebel proposed a schematic phase diagram, describing the structural evolution of Nafion as a function of hydration level.[42] However, our schematic diagram to understand the hydrated morphology of the hydrocarbon membrane with different crystallinity is different from the Gebel diagram. As shown in Scheme 2, in the case of HC-SPPS with increasing relative humidity, the ion−water aggregates start to develop and gradually become largest at some certain level of humidity, but after that, the water starts to disperse in the whole membrane. As described above, we consider the PPS crystallite domain in the membrane as a core−shell model. For HC-PPS membranes, initially the water is absorbed by the outside amorphous hydrophilic "shell" and gradually penetrates into the hydrophobic "core" of the crystallite domain, with developing some ion−water aggregates. The crystallize sizes in the HC-SPPS membranes are larger comparing with those of LC-SPPS, and we suggest that the larger crystallites assist forming large ion−water aggregates in HC-PPS. However, in the case of the LC-SPPS membrane, with increasing relative humidity, the water penetrates into the membrane but without forming any ion−water aggregates; the water starts to disperse and, at higher relative humidity, become completely dispersed in the membrane.

Conclusions

A fundamental study on the comparison of the structure and morphology of HC- and LC-SPPS membranes as electrolytes in PEFCs was made on the basis of experimental results. WAXS results showed a remarkable difference in the morphology of sulfonated membranes of HC- and LC-PPS. For the HC-PPS membrane, the crystallinity decreased steeply up to the ion-exchange capacity (IEC) of 1.6 meq/g, but in the case of the LC-PPS membrane, crystallinity decreased up to an IEC of 1.2 meq/g, but not so steeply like the HC membrane, and also became equilibrium comparatively earlier than HC-PPS membranes. The crystallite size of the HC-SPPS membranes was several times larger than that of LC-SPPS for the same IEC. HC-SPPS showed a broad shoulder crystalline peak in the SAXS profile at around 0.5 nm^{-1}, which was from the electron density difference between the lamellar crystallite domains and amorphous domains of the membrane, but the LC-SPPS did not show any crystalline shoulder peak in the lower-q region due to its lower crystallinity. No peak from ion−water aggregates appeared in the high-q region in the SAXS profiles for both HC- and LC-SPPS, which meant that the rigid backbone of PPS restricts the molecular mobility and rearrangement of main chains in both HC- and LC-SPPS membranes with varied amounts of water. From the Porod plots for HC- and LC-SPPS membranes, the intercept slope values of the SAXS profile at the higher-q region were found as around −6, which indicated that the polymer/water interface was not sharp, but remarkably

SCHEME 2: Three-Dimensional (3D) Schematic Diagram of States of Ion−Water Aggregates in the HC- and LC-SPPS Membranes under Varied Hydration Levels[a]

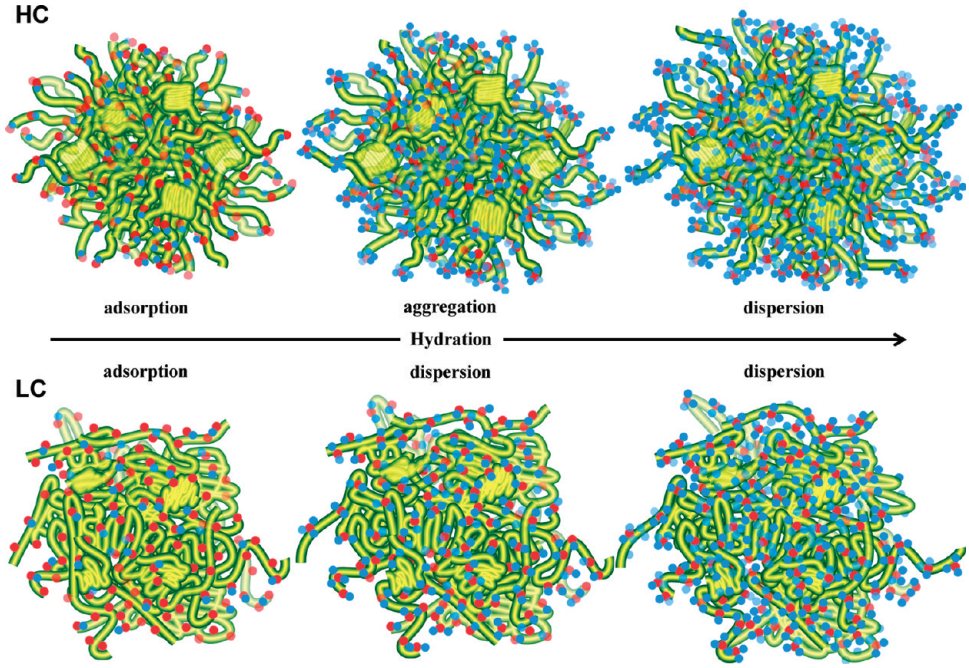

[a] For HC-SPPS membranes, the ion−water aggregates become larger with increasing RH, but after a certain hydration level, the ion−water aggregates start to become dispersed. For LC-SPPS, the ion−water aggregates disperse without making any larger ion−water aggregates with increasing RH.

diffused. Proton conductivities were almost identical for the same IEC membranes of HC- and LC-SPPS membranes.

Owing to its high crystallinity, the HC-SPPS membrane has better mechanical properties, and from the experimental results, we found that it has a tendency to develop ion−water aggregates at lower RH (up to 50% RH). From the fundamental study, we suggest that the PPS membrane is a high-performance PEM material, and among the two kinds of membranes studied, HC-SPPS will have better performance in PEFCs than LC-SPPS membranes.

Acknowledgment. This work was financially supported by the Ministry of Economy, Trade and Industry (METI) and the New Energy and Industrial Technology Development Organization (NEDO), Japan. We are grateful to KANEKA CORPORATION, Japan, for kindly providing the SPPS samples.

Supporting Information Available: Description and figures of water uptake and proton conductivity for HC-SPPS and LC-SPPS membranes in varied hydration conditions. This material is available free of charge via the Internet at http://pubs.acs.org.

References and Notes

(1) Appleby, A. J.; Foulkes, F. R. *Fuel Cell Handbook*; Van Nostrand Reinhold: New York, 1989.
(2) Carratte, L.; Friedlich, K. A.; Stimming, U. *Fuel Cells* **2001**, *1*, 5.
(3) Steele, C. H. B.; Heinzel, A. *Nature* **2001**, *414*, 345.
(4) Maier, G.; Haack, J. M. *Adv. Polym. Sci.* **2008**, *216*, 1.
(5) Roziere, J.; Jones, D. J. *Annu. Rev. Mater. Res.* **2003**, *33*, 503.
(6) Higashihara, T.; Matsumoto, K.; Ueda, M. *Polymer* **2009**, *50*, 5341.
(7) Soma, G.; Kyonsuku, M. *Polymer* **2009**, *50*, 1034.
(8) Schonherr, H.; Frank, C. W. *Macromolecules* **2003**, *36*, 1188.
(9) Despotopoulou, M. M.; Miller, R. D.; Rabolt, J. F.; Frank, C. W. *J. Polym. Sci., Part B: Polym. Phys.* **1996**, *34*, 2335.
(10) Zhu, L.; Cheng, S. Z. D.; Calhoun, B. H.; Ge, Q.; Quirk, R. P.; Thomas, E. L.; Hsiao, B. S.; Yeh, F. J.; Lotz, B. *J. Am. Chem. Soc.* **2000**, *122*, 5957.
(11) Sun, Y. S.; Chung, T. M.; Li, Y. J.; Ho, R. M.; Ko, B. T.; Jeng, U. S.; Lotz, B. *Macromolecules* **2006**, *39*, 5782.
(12) Quiram, D. J.; Register, R. A.; Marchand, G. R.; Adamson, D. H. *Macromolecules* **1998**, *31*, 4891.
(13) Huang, P.; Zhu, L.; Cheng, S. Z. D.; Ge, Q.; Quirk, R. P.; Thomas, E. L.; Lotz, B.; Hsiao, B. S.; Liu, L. Z.; Yeh, F. J. *Macromolecules* **2001**, *34*, 6649.
(14) Huang, P.; Guo, Y.; Quirk, R. P.; Ruan, J. J.; Lotz, B.; Thomas, E. L.; Hsiao, B. S.; Avila-Orta, C. A.; Sics, I.; Cheng, S. Z. D. *Polymer* **2006**, *47*, 5457.
(15) Liu, Y.; Cui, L.; Guan, F. X.; Gao, Y.; Hedin, N. E.; Zhu, L.; Fong, H. *Macromolecules* **2007**, *40*, 6283.
(16) Steinhart, M.; Senz, S.; Wehrspohn, R. B.; Gösele, U.; Wendorff, J. H. *Macromolecules* **2003**, *36*, 3646.
(17) Steinhart, M.; Göring, P.; Dernaika, H.; Prabhukaran, M.; Gösele, U.; Hempel, E.; Thurn-Albrecht, T. *Phys. Rev. Lett.* **2006**, *97*, 027801.
(18) Wu, H.; Wang, W.; Yang, H.; Su, Z. *Macromolecules* **2007**, *40*, 4244.
(19) Shin, K.; Woo, E.; Jeong, Y. G.; Kim, C.; Huh, J.; Kim, K. W. *Macromolecules* **2007**, *40*, 6617.
(20) Woo, E.; Huh, J.; Jeong, Y. G.; Shin, K. *Phys. Rev. Lett.* **2007**, *98*, 136103.
(21) Hu, Z. J.; Baralia, G.; Bayot, V.; Gohy, J. F.; Jonas, A. M. *Nano Lett.* **2005**, *5*, 1738.
(22) Loo, Y. L.; Register, R. A.; Ryan, A. J. *Phys. Rev. Lett.* **2000**, *84*, 4120.
(23) Massa, M. V.; Dalnoki-Veress, K. *Phys. Rev. Lett.* **2004**, *92*, 255509.
(24) Nojima, S.; Ohguma, Y.; Namiki, S.; Ishizone, T.; Yamaguchi, K. *Macromolecules* **2008**, *41*, 1915.
(25) Jiang, S. C.; Ji, X. L.; An, L. J.; Jiang, B. Z. *Polymer* **2001**, *42*, 3901.
(26) Schauer, J.; Kudelaa, V.; Richaub, K.; Mohr, R. *Desalination* **2006**, *198*, 256.
(27) Rajendra, K. K.; Jon, F. G.; Barbara, J. L. *Macromolecules* **2003**, *36*, 2907.
(28) Barique, M. A.; Wu, L.; Takimoto, N.; Kidena, K.; Ohira, A. *J. Phys. Chem. B* **2009**, *113*, 15921.
(29) Hidekazu, K.; Kiyoyuki, N. European Patent EP 1380 619A1, January 2004.
(30) King-Fu, L.; Horng-Long, C.; Yu-Hui, C. *Polymer* **2004**, *45*, 2387.
(31) Napolitano, R.; Pirozzi, B.; Salvione, A. *Macromolecules* **1999**, *32*, 7682.
(32) Ballirano, P.; Caminiti, R.; D'ilario, L.; Martinelli, A.; Piozzi, A.; Maras, A. *J. Mater. Sci.* **1998**, *33*, 3519.
(33) Hay, J. N.; Luck, D. A. *Polymer* **2001**, *42*, 8297.
(34) Swier, S.; Chun, Y. S.; Gasa, J.; Shaw, M. T.; Weiss, R. A. *Polym. Eng. Sci.* **2005**, *45*, 1081.
(35) Bailly, C.; Williams, D. J.; Karasz, F. E.; MacKnight, W. J. *Polymer* **1987**, *28*, 1009.
(36) Lu, S. X.; Capel, Cebe, P. *Macromolecules.* **1997**, *30*, 6243.
(37) Kannan, R.; Parthasarathy, M.; Maraveedu, S. U.; Kurungot, S.; Pillai, V. K. *Langmuir* **2009**, *25*, 8299.
(38) Fujimura, M.; Hashimoto, T.; Kawai, H. *Macromolecules* **1981**, *14*, 1309.
(39) Fujimura, M.; Hashimoto, T.; Kawai, H. *Macromolecules* **1982**, *15*, 136.
(40) Michael, E.; Alexei, A. K.; Eckhard, S. *Adv. Polym. Sci.* **2008**, *215*, 15.
(41) Sekhon, S. S.; Park, J. S.; Cho, E.; Yoon, Y.; Kim, C.; Lee, W. *Macromolecules* **2009**, *42*, 2054.
(42) Gebel, G. *Polymer* **2000**, *41*, 5829.

JP108562S